ORGANIC CHEMISTRY

Pd/Xu-Phos-catalyzed asymmetric elimination of fully substituted enol triflates into axially chiral trisubstituted allenes

Jie Han[1,2,3]†, Siyuan Liu[1]†, Huanan Wang[1], Jie Wang[1], Hui Qian[1], Zhiming Li[1]*, Shengming Ma[1,4]*, Junliang Zhang[1,2,3]*

The β-H elimination, as one of the most important elementary reactions in transition metal chemistry, is a key step in quenching the carbon-palladium bond for the Heck reaction. However, the β-H elimination of the alkenyl palladium species leading to allene is an energetically unfavored process, and therefore, it has been a long-standing challenge in control of this process via enantioselective manner. We developed a concise and efficient methodology to construct trisubstituted chiral allenes from stereodefined fully substituted enol triflates by the enantioselective β-H elimination of the alkenyl palladium species under mild conditions. The identified Xu-Phos play a crucial role in the chemoselectivity and enantioselectivity. Multiple linear regression analysis shows the important steric effect on enantioselectivity. DFT computation results allow us to propose an intramolecular base ($^{-}$OAc)–assisted deprotonation mechanism for this progress. Distortion-interaction and energy decomposition analysis indicate that the difference in electrostatic energy (E_{elec}) of the two intramolecular base-assisted deprotonation transition states dominates the stereoselectivity.

INTRODUCTION

The β-H elimination of alkyl metal species has emerged as a powerful strategy to construct alkenes (Fig. 1A) (*1*–*5*). In this regard, regioselective β-H elimination of alkyl bromides by Co (*6*, *7*) and Pd (*8*) catalysts has received increasing attention. In contrast, the β-H elimination of alkenyl palladium species remains a very challenging undertaking because it is an energetically unfavored process (Fig. 1A). In 1989, Tao and co-workers (*9*) reported the first example of synthesis of racemic allenes via the β-H elimination of alkenyl palladium species. Miura (*10*), Hamblett (*11*), Jazzar (*12*), Frantz (*13*), and Cheng (*14*) have also made seminal contributions in this field. On the other hand, axially chiral allenes have attracted attention from chemists due to their unique structure and reactivity. Undoubtedly, the exploration of a catalytic system that enables the synthesis of allenes, especially axially chiral allenes, is more attractive and challenging (Fig. 1A). Great efforts have been made to develop new methodologies for the preparation of optically active allenes (*15*–*18*), such as the organocatalytic (*19*, *20*), enzyme-catalytic (*21*, *22*) and metal-catalytic (*23*–*27*) transformations. In 2013, after an extensive screening of ~110 chiral phosphine ligands, Frantz and co-workers (*28*) demonstrated the first example of synthesis of disubstituted chiral allenoates via the Pd-catalyzed asymmetric β-H elimination of vinyl palladium species with the use of the homemade chiral ligand (Fig. 1A). However, the synthesis of electron-rich trisubstituted chiral allenes in high enantioselectivity was still challenging. Recently, Zhang and Ma have explored an alternative method for the synthesis of trisubstituted allenes via a Pd-catalyzed asymmetric Heck reaction of aryl triflates with internal alkynes (*29*). In most cases, the symmetric internal alkynes were used to avoid the regioselectivity issue. During the course of this study, we became interested in Pd-catalyzed asymmetric direct elimination of fully substituted enol triflates to modularized synthesis of various trisubstituted axially chiral allenes under mild conditions, in which there is no regioselectivity issue (Fig. 1B). However, several challenging issues should be addressed (Fig. 1B, bottom): (i) Allene product might undergo further isomerization to 1,3-diene by-product via anti-regioselective hydropalladation of the allene followed by a second β-H elimination (*30*); (ii) the further carbopalladation of the alkenyl palladium species with the allene product might occur, resulting in various by-products (*31*–*35*); (iii) how to gain high enantioselectivity; and (iv) the β-H elimination of the in situ generated alkenyl palladium species is an energetically unfavored process, which often makes the substrate scope narrow (*9*–*14*). Combined with the reported literature and our previous work, we firmly believe that the ligand is the key to address these issues. Last, multiple linear regression (MLR) analysis also shows that the steric hindrance of the ligand is a key factor in high enantioselectivity.

RESULTS

Reaction development

A series of commercially available chiral ligands were first examined with **1a** as the model substrate (Fig. 2). Frantz's ligand **L1** was first tested and found to be ineffective, delivering the desired allene in only 5% yield with 43:57 enantio ratio (er), indicating that the β-H elimination of the electron-rich alkenyl palladium species is much more challenging than that of the electron-deficient one. Other commonly used chiral ligands **L2** to **L5** such as

[1]Department of Chemistry, Fudan University, Shanghai 200438, China. [2]Zhuhai Fudan Innovation Institute, Zhuhai 519000, China. [3]Shanghai Key Laboratory of Green Chemistry and Chemical Processes, Department of Chemistry, East China Normal University, 3663 N. Zhongshan Road, Shanghai 200062, China. [4]State Key Laboratory of Organometallic Chemistry, Shanghai Institute of Organic Chemistry, CAS, Shanghai, China.
†These authors contributed equally to this work.
*Corresponding author. Email: junliangzhang@fudan.edu.cn (J.Z.); masm@mail.sioc.ac.cn (S.M.); zmli@fudan.edu.cn (Z.L.)

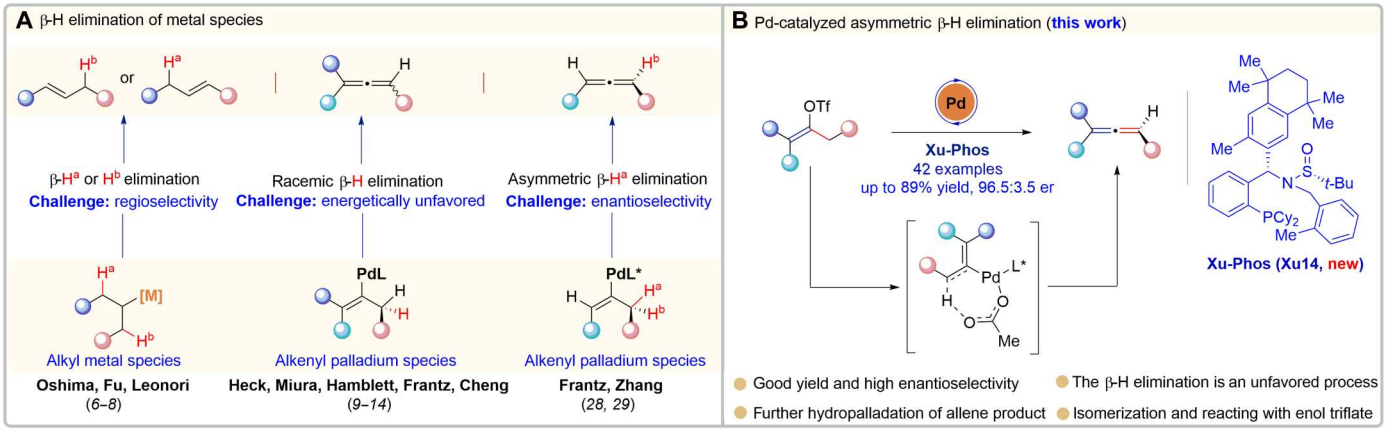

Fig. 1. Background and reaction design. (**A**) β-H elimination of alkyl metal species and β-H elimination of vinyl palladium species. (**B**) This work: Pd-catalyzed asymmetric elimination of fully substituted enol triflates en route to trisubstituted chiral allenes.

Duphos, QuinoxP, Pybox, and (*R*)-*N*,*N*-dimethyl-1-[(*S*)-2-(diphenylphosphino)ferrocenyl]ethylamine (PPFA) all failed to promote the reaction. The phosphoramidite **L6** also furnished the product in low yield with 61.5:38.5 er (for other more ligands and results, see fig. S1). We next turned to the sulfinamide-phosphine ligands (**Sadphos**) developed by our group, which have emerged as powerful ligands in various asymmetric catalyses (*36*–*40*), especially for the asymmetric palladium catalysis. Unfortunately, **Ming-Phos**, **Xiang-Phos**, and **Xu-Phos** could not furnish the desired product **2a** either. To our delight, ***N*-Me-Xu-Phos** (**Xu1**) could give a promising result, obtaining **2a** in 32% yield with 66.5:33.5 er. In addition, we found that the corresponding **Xu-Phos** with a free NH moiety had no reactivity, indicating that the *N*-methyl group could improve the catalytic activity of the catalyst.

Comparing the different results from **Xu-Phos** and ***N*-Me-Xu-Phos**, we envisaged that fine-tuning the substituent of **Xu-Phos**, especially the *N*-substituent, may have a notable impact on catalytic activity and the enantioselectivity. Thus, we prepared a variety of **Xu-Phos** with different substituents and investigated their performances in the asymmetric β-H elimination (Fig. 2). The tuning of the *N*-substituent (R) of **Xu-Phos** (**Xu2** to **Xu6**) was first carried out, among them **Xu6** with *N*-2-methylbenzyl group could deliver the desired allene **2a** in 61% yield and 83.5:16.5 er. Note that the fine-tuning of the *N*-substituent of the **Xu-Phos** led to a substantial effect on enantioselectivity. For example, using **Xu6** (R = 2-methylbenzyl) instead of **Xu2** (R = Bn) increased the er value of **2a** from 72:28 to 83.5:16.5. Next, the variation of the aryl group, structured as **Xu7** to **Xu10**, did not improve the enantioselectivity. Further tuning *N*-substituent did not bring better enantioselectivity (**Xu11** to **Xu13**). When the temperature was decreased to 50°C, **2a** was delivered in 63% yield with 86:14 er (Fig. 2, entry 1). The yield was further improved to 74% by reducing the amount of water (Fig. 2, entry 3). Further base screening did not give better results (Fig. 2, entries 4 and 5). Other reaction parameters were also investigated and summarized in the Supplementary Materials (tables S1 to S3).

Second round screening and modification of **Xu-Phos** were then conducted. The enantiomeric ratio was further improved to 94:6 with **Xu14** as the ligand, but the reaction became much slower. Further changing the steric hindrance of ligands (**Xu15** to **Xu19**) resulted in lower er values. The yield was improved to 72% under the condition of $Pd_2(dba)_3$ [5 mole percent (mol %)], **Xu14** (12 mol %), and *N*,*N*-diisopropylethylamine [DIPEA (0.4 mmol)] in *i*-PrOAc (0.5 ml) for 45 hours. Next, we turned to investigate other palladium precursors, reaction temperature, and solvents. The yield could be improved to 60% when $Pd(OAc)_2$ was used instead of $Pd_2(dba)_3$ (Fig. 2, entry 6). The reaction worked smoothly at 25°C, delivering the product **2a** in 68% yield with 93:7 er under the catalysis of $Pd(OAc)_2$/**Xu14** (Fig. 2, entry 7). The solvents were tested, and the use of *i*-Pr_2O increased the er value to 95:5 (Fig. 2, entries 8 and 9). The optimal reaction conditions were identified as 5 mol % of $Pd(OAc)_2$, 7.5 mol % of **Xu14**, and a mixed base of DIPEA (2.0 equiv) and Na_2CO_3 (1.0 equiv) in *i*-Pr_2O at 25°C, affording the desired allene **2a** in 87% nuclear magnetic resonance (NMR) yield with 95:5 er (Fig. 2, entry 10). When DIPEA or Na_2CO_3 was used as the base, the reaction delivered **2a** in lower yields (Fig. 2, entries 11 and 12). We found that allene product could undergo subsequent isomerization to form the 1,3-diene product **3a** (for details, please see the Supplementary Materials and tables S2 and S7). After an extensive screening of **Xu-Phos** (**Xu20** to **Xu38**), we finally identified that **Xu14** is responsible for the good yields with high enantiomeric ratios (fig. S2). The absolute configuration of **Xu-Phos** was confirmed via x-ray diffraction analysis of **Xu14** and **Xu22**.

Next, we sought to understand which structural features of the chiral ligands are responsible for the enantioselectivity. In particular, 16 chiral ligands (**Xu14** and **Xu-Phos** with aryl substituents similar to **Xu14**; fig. S3) were numerically parameterized, and an MLR (*41*–*45*) model between parameters and reaction enantioselectivity ($\Delta\Delta G^{\ddagger}$) was constructed using IBM SPSS Statistics 20 software (Fig. 3A, left). In view of the complex flexible structure and multicoordination nature of the ligands, an extensive conformational search for the Pd(0)–**Xu-Phos** complexes was conducted. Seventy-six parameters including both Boltzmann-weighted (Boltz) and lowest-energy (LE) conformational parameters are obtained from density functional theory (DFT) calculations (fig. S5 and table S11). The detailed strategies of conformational search and DFT calculation can be found in the Supplementary Materials. The MLR model features the steric effects as the important factor. The parameters include Sterimol parameters (*46*, *47*) $\mathbf{B_1(R^3)^{Boltz}}$

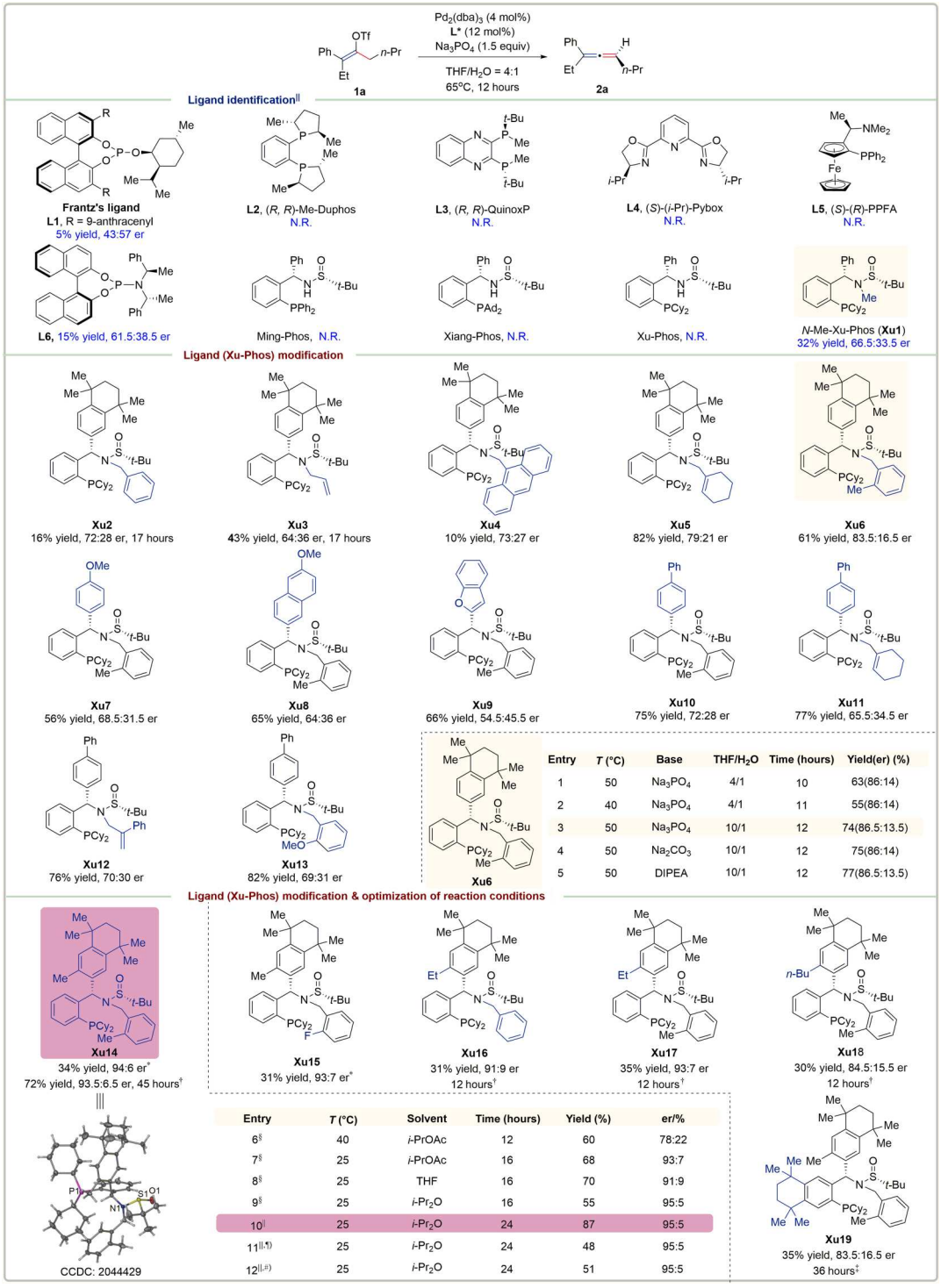

Fig. 2. Optimization of reaction conditions. Reaction conditions: **1a** (0.1 mmol), $Pd_2(dba)_3$ (4 mol %), ligand (12 mol %), and Na_3PO_4 (0.15 mmol) in THF/H_2O (4/1) (0.5 ml) at 65°C under N_2 atmosphere. *THF/H_2O (10/1) (0.5 ml) at 50°C. †$Pd_2(dba)_3$ (5 mol %), DIPEA (0.4 mmol), and *i*-PrOAc (0.5 ml) were used. ‡40°C. §$Pd(OAc)_2$ (10 mol %), **Xu14** (12 mol %), and DIPEA (0.4 mmol). ‖$Pd(OAc)_2$ (5 mol %), **Xu14** (7.5 mol %), DIPEA (0.2 mmol), and Na_2CO_3 (0.1 mmol) were used. ¶No DIPEA. #No Na_2CO_3. The yields with CH_2Br_2 as an internal standard were determined by ^1H NMR, and er values were determined by high-performance liquid chromatography analysis.

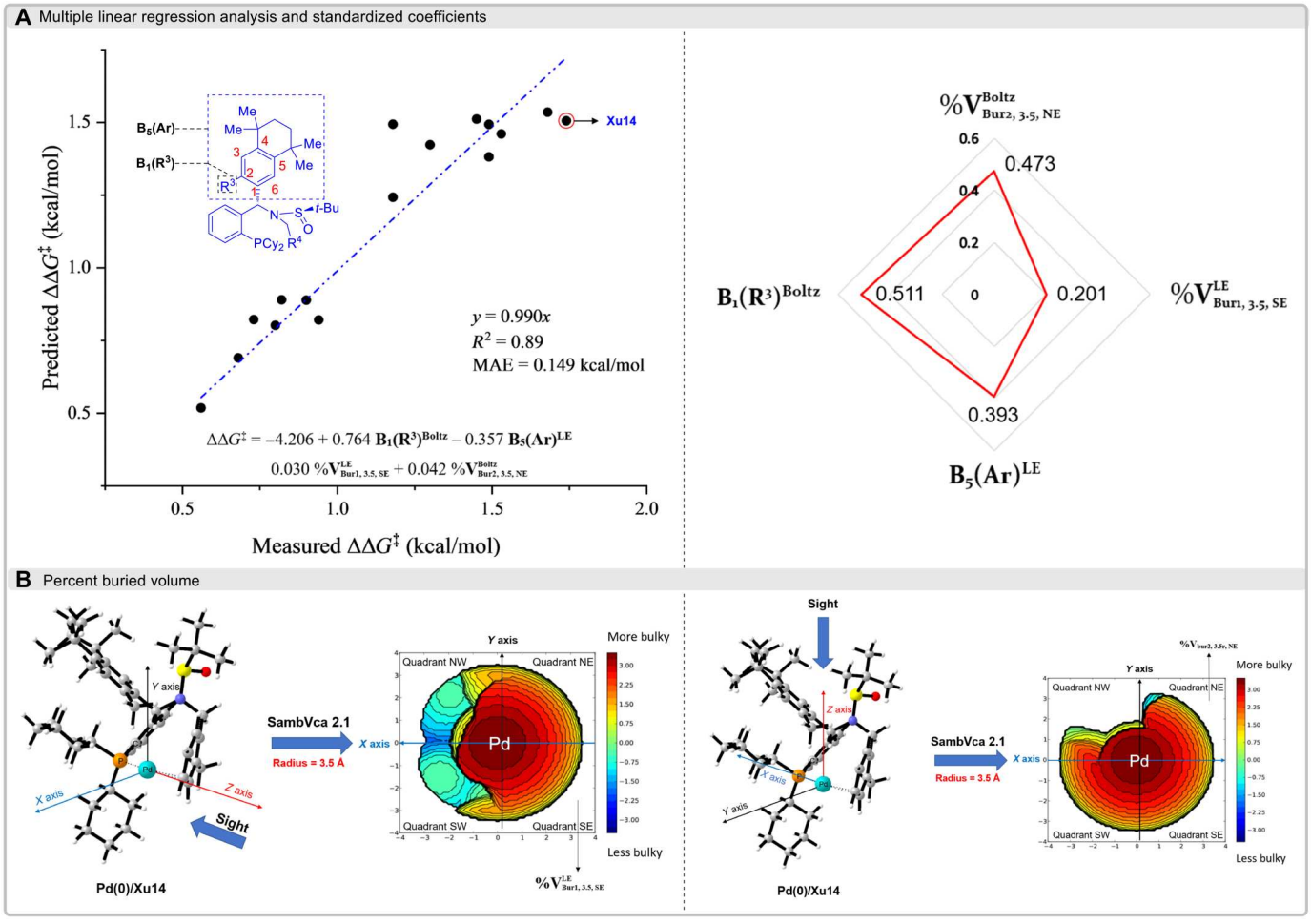

Fig. 3. MLR analysis and descriptors used in MLR analysis. (**A**) MLR analysis and standardized coefficients. (**B**) Percent buried volume obtained using SambVca 2.1 (see the Supplementary Materials for details).

($\mathbf{R^3}$'s minimum width) and $\mathbf{B_5(Ar)^{LE}}$ (Ar's maximum width) and percent buried volume [$\%\mathbf{V_{bur1}(SE)^{LE}}$ and $\%\mathbf{V_{bur2}(NE)^{Boltz}}$, steric effect of $\mathbf{R^3}$ and $\mathbf{R^4}$] (*48*–*50*), calculated by SambVca (Fig. 3B) (*49*, *50*). $\mathbf{B_1(R^3)^{Boltz}}$, $\%\mathbf{V_{bur1}(SE)^{LE}}$, and $\%\mathbf{V_{bur2}(NE)^{Boltz}}$ are positively correlated with $\Delta\Delta G^{\ddagger}$, while $\mathbf{B_5(Ar)^{LE}}$ is negatively correlated. The coefficient of each parameter was normalized (Fig. 3A, right), and the results show that $\mathbf{B_1(R^3)^{Boltz}}$ has the greatest influence (0.511) on $\Delta\Delta G^{\ddagger}$.

Substrate scope of the substrate

With the optimal reaction conditions established, we then turned to examine the substrate scope via the variation of the aryl group of enol triflates **1** (Fig. 4, **2a** to **2t**). A variety of fully substituted (*Z*)-enol triflates with electron-neutral and electron-rich aryl moieties that all worked smoothly to afford the corresponding products with high er (**2a** to **2n**) but lower reactivity was observed with the electron-deficient group (**2l**). The reaction of those enol triflates with electron-deficient groups such as *meta*-Cl and CF_3 at the phenyl ring required a higher amount of catalyst [10 mol % $Pd(OAc)_2$ and 15 mol % **Xu14**] and longer reaction time (**2l**, **2o**, and **2p**). The disubstituted aryl group was also well compatible, delivering **2q** in 85% yield with 96:4 er. The phenyl group could be replaced by other aryl or heteroaryl groups such as 2,3-dihydrobenzofuran-5-yl (**2r**), benzo[*d*][1,3]dioxol-5-yl (**2s**), and 2-naphthyl (**2t**); all of them could furnish the desired allene products in 68 to 82% yields with 95:5 to 96.5:3.5 er.

Subsequently, we studied the reaction scope by variation of R^1 and R^2, as well as the aryl group of enol triflates (Fig. 4, **2u** to **2pp**). For linear aliphatic R^1, e.g., Me, *n*-Pr, *n*-Bu, and so on, the corresponding products **2u** to **2dd** were obtained in 72 to 89% yields with 92:8 to 95:5 er. Meanwhile, the absolute configuration of the products was further confirmed by the known allene **2cc** (*29*). The functional groups such as CF_3 (**2ee**), F (**2ff**), alkenyl (**2gg**), and Ph (**2hh**) were all tolerated. Specifically, increasing the steric hindrance of R^1 group would make the reaction slower with relatively lower yield (**2ii** to **2kk**). The allene product **2ll** was obtained in 86% yield with 88:12 er when R^2 is the methyl group. It was interesting to find that with a longer linear aliphatic R^2, the desired allene could be furnished in 78 to 88% yields with 95:5 to 96:4% er (**2mm** to **2pp**). These results reveal that the R^2 group, which is close to the eliminate β-H, affects the enantioselectivity a bit.

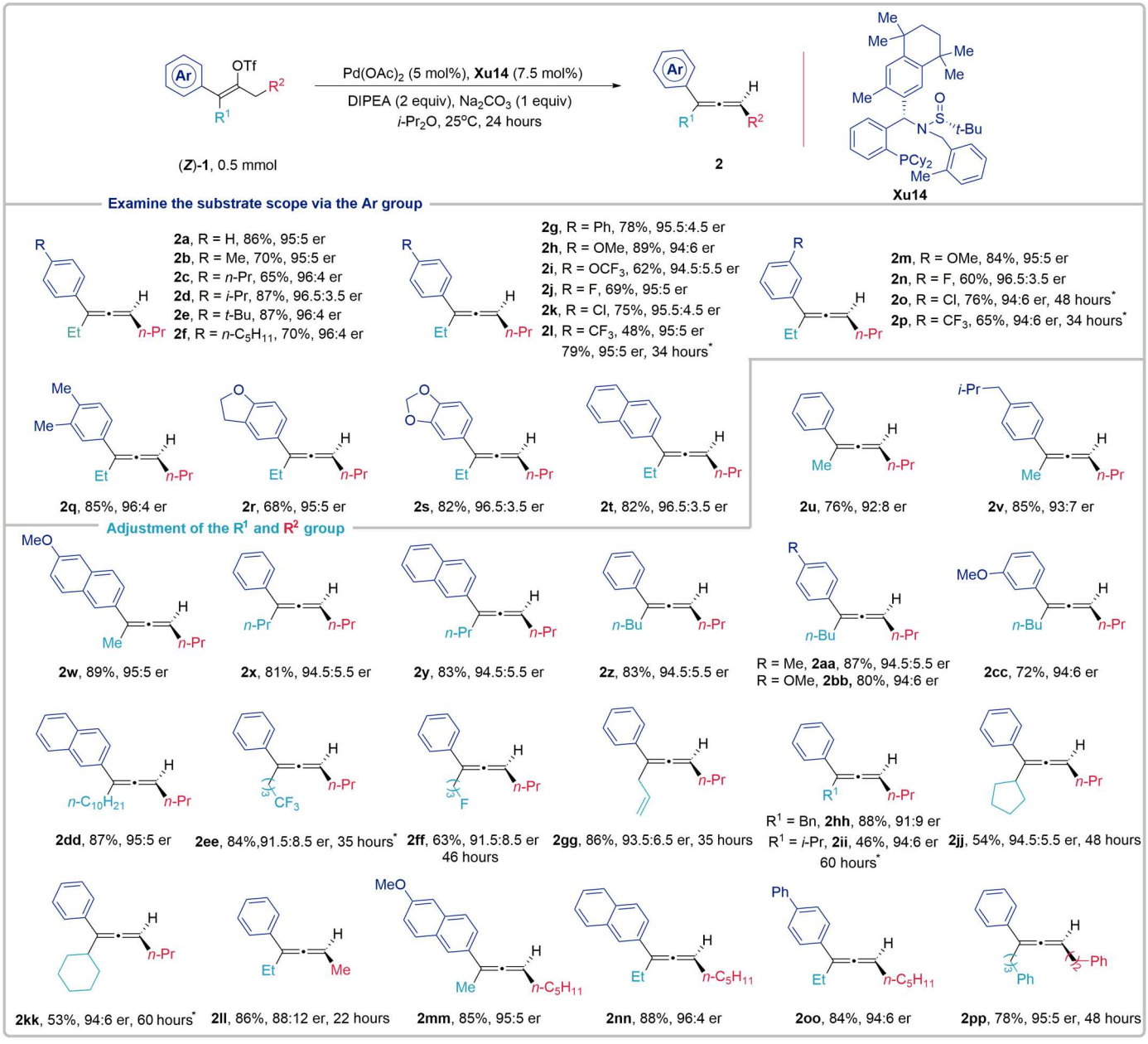

Fig. 4. Exploration of the substrate scope. *$Pd(OAc)_2$ (10 mol %) and **Xu14** (15 mol %) were used.

Mechanistic investigation

To show the synthetic practicability of our method, we demonstrated a gram-scale synthesis (Fig. 5A). The reaction of 7 mmol of **1a** worked smoothly under the catalysis of only 1 mol % of $Pd(OAc)_2$, delivering 1.05 g of **2a** in 81% yield without loss of the enantioselectivity. An efficient Rh(III)-catalyzed allylation of *N*-methoxybenzamide with **2a** produced the compound **3b** in 76% yield with 95:5 er, indicating that the axial chirality could be well transferred to the carbon stereocenter (Fig. 5B) (*51*). To deeply understand the reaction mechanism (*12*, *52*, *53*), DFT calculations were carried out with the Gaussian 09 software package (*54*–*57*). Calculation details were provided in the Supplementary Materials. The free-energy reaction profiles are shown in Fig. 5C. Coordination of (*Z*)-**1a** with Pd(0)-**Xu14** forms complex **A**. This process is endothermic because of the entropy penalty. Then, **A** undergoes oxidative addition reaction via **TS A/B** to give complex **B**. The activation barrier is only 3.5 kcal/mol. Note that the coordination of $^{-}$OAc with palladium can reduce the barrier of this process. Without acetate involved, oxidative addition needs to overcome a barrier of 11.3 kcal/mol (fig. S6A). For the subsequent deprotonation, complex **B** undergoes conformational transformation to complex **C** and **C′**. Through **TS C/D** and **TS C′/D′**, the intramolecular base ($^{-}$OAc)–assisted deprotonation processes were carried out to generate **D, D′,** and acetic acid, wherein **D** and **D′** are complexes of Pd(0)-**Xu14** coordinated with product **2a** and its enantiomer. Then, acetic acid reacts with Na_2CO_3 to regenerate $^{-}$OAc for the next catalytic cycle. The barriers

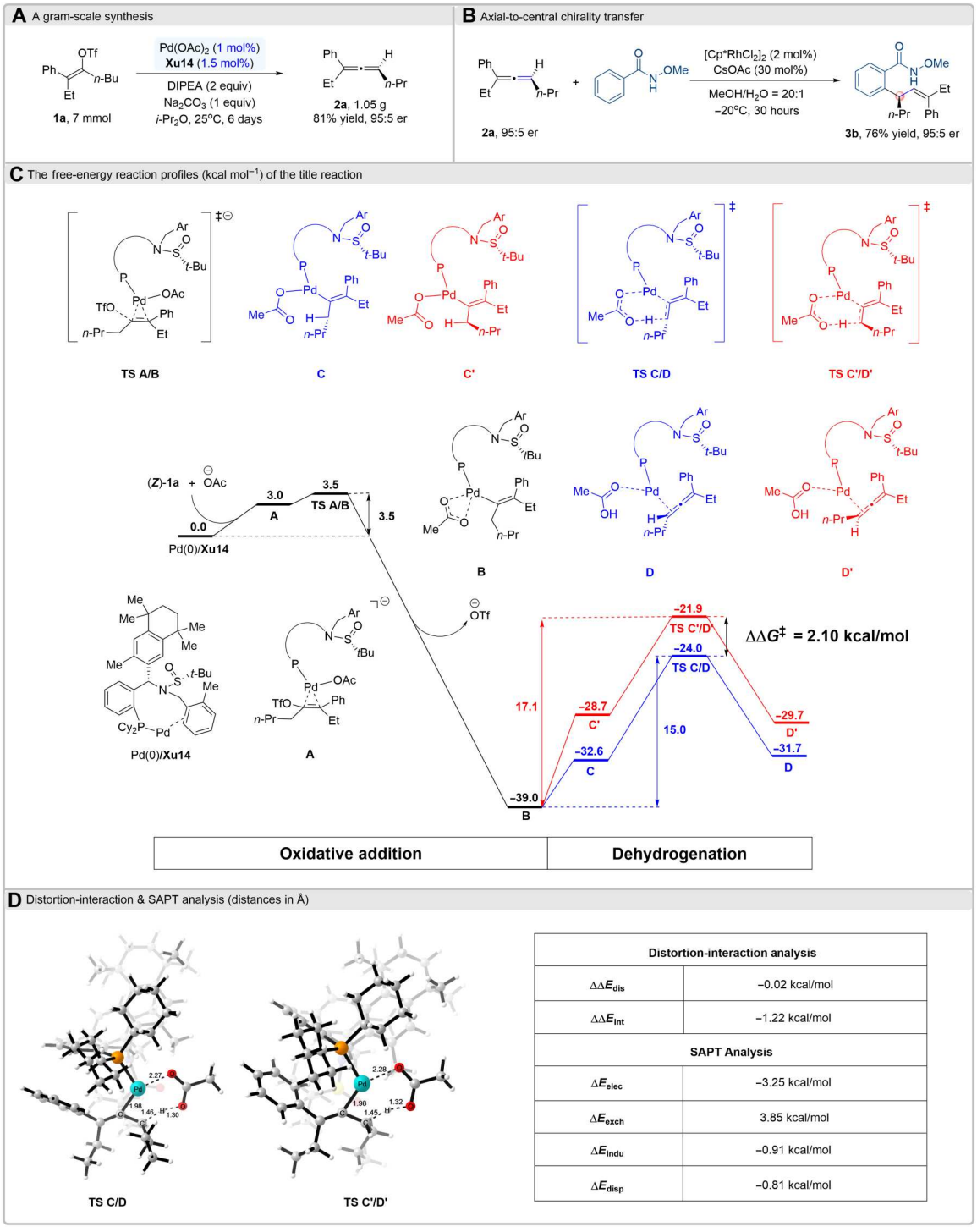

Fig. 5. Synthetic applications and DFT calculations. (**A**) A gram-scale synthesis. (**B**) Axial-to-central chirality transfer. (**C**) The free-energy reaction profiles (kcal mol^{-1}) of the title reaction. (**D**) Distortion-interaction and symmetry-adapted perturbation theory (SAPT) analysis (distances in Å).

of 15.0 kcal/mol and 17.1 kcal/mol need to be surmounted for the deprotonation process, respectively, indicating that this step is both enantiodetermining and rate-determining. The $\Delta\Delta G^{\ddagger}$ between **TS C/D** and **TS C′/D′** is 2.10 kcal/mol, which is in good agreement with the experimental results (95:5 er).

The syn β-H elimination pathway with activation barrier at 17.1 kcal/mol via **TS C/D_PdH** is less likely due to the higher energy demand (fig. S6A), while the possibility cannot be completely excluded. Whether the dehydrogenation mechanism is a base-assisted deprotonation or a syn β-H elimination mechanism depends on the alkalinity of the paired negative ions of the Pd salt used. When palladium acetate was used, the β-H elimination barrier is 2.1 kcal/mol higher than that of the base-assisted dehydrogenation (fig. S6B). However, as $Pd(CF_3COO)_2$ was used, because of the weak alkalinity of trifluoroacetate, the β-H elimination mechanism of Pd is more favored than the base-assisted dehydrogenation (fig. S6C). We have also envisaged the $^{-}NaCO_3$ instead of ^{-}OAc to participate in this process as base. Although the alkalinity of $^{-}NaCO_3$ is stronger than that of ^{-}OAc, the solubility of Na_2CO_3 in the system was not good. Thus, the intramolecular base (^{-}OAc)–assisted deprotonation mechanism was finally adopted.

To explore the origin of high enantioselectivity, distortion-interaction analysis (*58*–*64*) was performed on **TS C/D** and **TS C′/D′**, respectively, with intermediate **B** as a reference (Fig. 5D). We divided the relevant structures into two parts: substrate and catalyst. The analysis results show that the distortion energy ΔE_{dis} of the two **TS**s are almost the same, and the difference is mainly in the interaction energy ΔE_{int}, indicating that ΔE_{int} may determine the enantioselectivity of the title reaction. In addition, although ΔE_{dis} of the two **TS**s are almost the same, the contributions from different parts are different. In **TS C/D**, the catalyst part $\Delta E_{dis\text{-}cat}$ contributes less and the substrate part $\Delta E_{dis\text{-}sub}$ contributes more, while it is vice versa in **TS C′/D′** (fig. S7). To explore the weak interaction energy in the two **TS**s, the symmetry-adapted perturbation theory (SAPT) (*65*) analysis was carried out at the SAPT0/def2-TZVP (*66*, *67*) level using the PSI4 program package (Fig. 5D) (*68*). The energy decomposition analysis suggested that the total interaction energy of **TS C/D** is lower than that of **TS C′/D′**, which is in line with the results of distortion-interaction analysis, and electrostatic energy (E_{elec}) dominates the stereoselectivity of the title reaction.

DISCUSSION

In summary, it has been a long-standing challenge to achieve trisubstituted allenes via the energetically unfavored β-H elimination of alkenyl palladium species in an enantioselective manner. We have developed an efficient Pd/**Xu-Phos** catalyzed asymmetric elimination of fully substituted enol triflates, delivering trisubstituted chiral allenes in up to 89% yield and 96.5:3.5 er under mild conditions. The identified **Xu14** through systemic fine-tuning is responsible for the good yields and high ers. It is worth emphasizing that this chiral ligand could be easily synthesized from readily available starting materials in short steps. Ongoing studies within our laboratory include the development of new methods for the construction of axial chirality via the stereoselective elimination of the vinyl palladium species. MLR analysis shows the important steric effect of $\mathbf{R^3}$ and $\mathbf{R^4}$ on enantioselectivity. Mechanistic investigations and DFT calculations allow us to propose an intramolecular base (^{-}OAc)–assisted deprotonation mechanism for this pathway. Distortion-interaction analysis and energy decomposition analysis indicate that the difference in E_{elec} dominates the stereoselectivity of this progress.

MATERIALS AND METHODS

General procedure for synthesis of chiral allenes

Under nitrogen atmosphere, a sealed tube (20 ml) with a magnetic stirring bar was charged with $Pd(OAc)_2$ (0.025 mmol) and **Xu14** (0.038 mmol). The tube was evacuated and backfilled with nitrogen three times. *i*-Pr_2O (2.5 ml) was added and stirred at room temperature for 1 hour. Then, enol triflate **1** (0.5 mmol), DIPEA (1 mmol), and Na_2CO_3 (0.5 mmol) were added to the reaction tube under a nitrogen atmosphere. The reaction mixture was evacuated and backfilled with nitrogen three times at −196°C. The mixture was warmed to room temperature. The reaction mixture was continuously stirred at 25°C. After the completion of the reaction monitored by thin-layer chromatography, the solvent was removed in a rotary evaporator and the residue was purified by flash column chromatography with *n*-hexane as eluent to give the desired product **2**.

Supplementary Materials

This PDF file includes:

Supplementary Text
Figs. S1 to S7
Tables S1 to S12
References

REFERENCES AND NOTES

1. G. Wilkillson, The long search for stable transition metal alkyls. *Science* **185**, 109–112 (1974).
2. S. K. Murphy, J. W. Park, F. A. Cruz, V. M. Dong, Rh-catalyzed C–C bond cleavage by transfer hydroformylation. *Science* **347**, 56–60 (2015).
3. S. Kusumoto, T. Tatsuki, K. Nozaki, The retro-hydroformylation reaction. *Angew. Chem. Int. Ed.* **54**, 8458–8461 (2015).
4. X. Fang, P. Yu, B. Morandi, Catalytic reversible alkene-nitrile interconversion through controllable transfer hydrocyanation. *Science* **351**, 832–836 (2016).
5. J. Hu, M. Wang, X. Pu, Nickel-catalysed retro-hydroamidocarbonylation of aliphatic amides to olefins. *Nat. Commun.* **8**, 14993 (2017).
6. T. Kobayashi, H. Ohmiya, H. Yorimitsu, K. Oshima, Cobalt-catalyzed regioselective dehydrohalogenation of alkyl halides with dimethylphenylsilylmethylmagnesium chloride. *J. Am. Chem. Soc.* **130**, 11276–11277 (2008).
7. H. Zhao, A. J. McMillan, T. Constantin, R. C. Mykura, F. Juliá, D. Leonori, Merging halogen-atom transfer (XAT) and cobalt catalysis to override E2-selectivity in the elimination of alkyl halides: A mild route toward contra-thermodynamic olefins. *J. Am. Chem. Soc.* **143**, 14806–14813 (2021).
8. A. C. Bissember, A. Levina, G. C. Fu, A mild, palladium-catalyzed method for the dehydrohalogenation of alkyl bromides: Synthetic and mechanistic studies. *J. Am. Chem. Soc.* **134**, 14232–14237 (2012).
9. W. Tao, L. J. Silverberg, A. L. Rheingold, R. F. Heck, Alkyne reactions with arylpalladium compounds. *Organometallics* **8**, 2550–2559 (1989).
10. S. Pivsa-Art, T. Satoh, M. Miura, M. Nomura, Palladium-catalyzed reaction of aryl bromides with dialkylacetylenes to produce allenic compounds. *Chem. Lett.* **26**, 823–824 (1997).
11. L. M. Chapman, B. Adams, L. T. Kliman, A. Makriyannis, C. L. Hamblett, Intramolecular Heck reactions of aryl chlorides with alkynes. *Tetrahedron Lett.* **51**, 1517–1522 (2010).
12. N. Nella, E. Parker, J. Hitce, P. Larini, R. Jazzar, O. Baudoin, Efficient Pd-catalyzed allene synthesis from alkynes and aryl bromides through an intramolecular base-assisted deprotonation (iBAD) mechanism. *Chem. A Eur. J.* **20**, 13272–13278 (2014).
13. R. Neff, D. Frantz, Cationic alkynyl Heck reaction toward substituted allenes using bobCat: A new hybrid Pd(0)-catalyst incorporating a water-soluble dba ligand. *J. Am. Chem. Soc.* **140**, 17428–17432 (2018).

14. W. Lv, Y. Chen, Z. Zhao, S. Wen, G. Cheng, Palladium-catalyzed regioselective Heck coupling of alkynes with aryl iodides for the synthesis of trisubstituted allenes. *Org. Lett.* **21**, 7795–7798 (2019).
15. M. Ogasawara, Catalytic enantioselective synthesis of axially chiral allenes. *Tetrahedron Asymmetry* **20**, 259–271 (2009).
16. R. K. Neff, D. E. Frantz, Recent advances in the catalytic syntheses of allenes: A critical assessment. *ACS Catal.* **4**, 519–528 (2014).
17. W. Chu, Y. Zhang, J. Wang, Recent advances in catalytic asymmetric synthesis of allenes. *Cat. Sci. Technol.* **7**, 4570–4579 (2017).
18. X. Huang, S. Ma, Allenation of terminal alkynes with aldehydes and ketones. *Acc. Chem. Res.* **52**, 1301–1312 (2019).
19. X. Li, J. Sun, Organocatalytic enantioselective synthesis of chiral allenes: Remote asymmetric 1,8-addition of indole imine methides. *Angew. Chem. Int. Ed.* **59**, 17049–17054 (2020).
20. J. Wang, S. Zheng, S. Rajkumar, J. Xie, N. Yu, Q. Peng, X. Yang, Chiral phosphoric acid-catalyzed stereodivergent synthesis of trisubstituted allenes and computational mechanistic studies. *Nat. Commun.* **11**, 5527 (2020).
21. J. Deska, J. Bäckvall, Enzymatic kinetic resolution of primary allenic alcohols. Application to the total synthesis and stereochemical assignment of stria-tisporolide A. *Org. Biomol. Chem.* **7**, 3379–3381 (2009).
22. C. Sapu, J. Bäckvall, J. Deska, Enantioselective enzymatic desymmetrization of prochiral allenic diols. *Angew. Chem. Int. Ed.* **50**, 9731–9734 (2011).
23. W.-D. Chu, L. Zhang, Z. Zhang, Q. Zhou, F. Mo, Y. Zhang, J. Wang, Enantioselective synthesis of trisubstituted allenes *via* Cu(I)-catalyzed coupling of diazoalkanes with terminal alkynes. *J. Am. Chem. Soc.* **138**, 14558–14561 (2016).
24. Y. Huang, J. Pozo, S. Torker, A. Hoveyda, Enantioselective synthesis of trisubstituted allenyl–B(pin) compounds by phosphine–Cu-catalyzed 1,3-enyne hydroboration. Insights regarding stereochemical integrity of Cu-allenyl intermediates. *J. Am. Chem. Soc.* **140**, 2643–2655 (2018).
25. W.-F. Zheng, W. Zhang, C. Huang, P. Wu, H. Qian, L. Wang, Y.-L. Guo, S. Ma, Tetrasubstituted allenes *via* the palladium-catalysed kinetic resolution of propargylic alcohols using a supporting ligand. *Nat. Catal.* **2**, 997–1005 (2019).
26. L. Bayeh-Romero, S. L. Buchwald, Copper hydride catalyzed enantioselective synthesis of axially chiral 1,3-disubstituted allenes. *J. Am. Chem. Soc.* **141**, 13788–13794 (2019).
27. C.-Y. He, Y.-X. Tan, X. Wang, R. Ding, Y.-F. Wang, F. Wang, D. Gao, P. Tian, G.-Q. Lin, Copper(I)-catalyzed diastereo- and enantio-selective construction of optically pure exocyclic allenes. *Nat. Commun.* **11**, 4293 (2020).
28. I. T. Crouch, R. K. Neff, D. E. Frantz, Pd-catalyzed asymmetric β-hydride elimination en route to chiral allenes. *J. Am. Chem. Soc.* **135**, 4970–4973 (2013).
29. C.-H. Zhu, H.-K. Chu, G. Li, S. Ma, J. Zhang, Pd-catalyzed enantioselective Heck reaction of aryl triflates and alkynes. *J. Am. Chem. Soc.* **141**, 19246–19251 (2019).
30. I. T. Crouch, T. Dreier, D. E. Frantz, Palladium-catalyzed elimination/isomerization of enol triflates into 1,3-dienes. *Angew. Chem. Int. Ed.* **50**, 6128–6132 (2011).
31. B. Friess, B. Cazes, J. Goré, Vinyl trifluorosulfonates in the carbopalladation of allenic hydrocarbons. *Tetrahedron Lett.* **29**, 4089–4092 (1988).
32. N. Vicart, B. Cazes, J. Goré, Synthesis of α or β-aminodienes via the carbopalladation of 1,2-propadiene. *Tetrahedron Lett.* **36**, 5015–5018 (1995).
33. R. Zimmer, C. U. Dinesh, E. Nandanan, F. A. Khan, Palladium-catalyzed reactions of allenes. *Chem. Rev.* **100**, 3067–3126 (2000).
34. H. Luo, Y. Zhao, D. Wang, M. Wang, Z. Shi, Stereoselective fluoroarylation of 1,1-difluoroallenes enabled by palladium catalysis. *Green Synth. Catal.* **1**, 134–142 (2020).
35. L. E. Vine, J. M. Schomaker, Pd-catalyzed Heck-type reactions of allenes for stereoselective syntheses of substituted 1,3-dienes. *Chem. A Eur. J.* **28**, e202103507 (2022).
36. H. Wang, H. Luo, Z.-M. Zhang, W.-F. Zheng, Y. Yin, H. Qian, J. Zhang, S. Ma, Pd-catalyzed enantioselective syntheses of trisubstituted allenes *via* coupling of propargylic benzoates with organoboronic acids. *J. Am. Chem. Soc.* **142**, 9763–9771 (2020).
37. L. Wang, K. Zhang, Y. Wang, W. Li, M. Chen, J. Zhang, Enantioselective synthesis of isoxazolines enabled by palladium-catalyzed carboetherification of alkenyl oximes. *Angew. Chem. Int. Ed.* **59**, 4421–4427 (2020).
38. Z.-M. Zhang, B. Xu, L. Wu, L. Zhou, D. Ji, Y. Liu, Z. Li, J. Zhang, Palladium/XuPhos-catalyzed enantioselective carboiodination of olefin-tethered aryl iodides. *J. Am. Chem. Soc.* **141**, 8110–8115 (2019).
39. L. Wang, M. Chen, P. Zhang, W. Li, J. Zhang, Palladium/PC-phos-catalyzed enantioselective arylation of general sulfenate anions: Scope and synthetic applications. *J. Am. Chem. Soc.* **140**, 3467–3473 (2018).
40. J. Han, W. Zhou, P.-C. Zhang, H. Wang, R. Zhang, H.-H. Wu, J. Zhang, Design and synthesis of WJ-Phos, and application in Cu-catalyzed enantioselective boroacylation of 1,1-disubstituted allenes. *ACS Catal.* **9**, 6890–6895 (2019).
41. K. B. Lipkowitz, M. Pradhan, Computational studies of chiral catalysts: A comparative molecular field analysis of an asymmetric diels–alder reaction with catalysts containing bisoxazoline or phosphinooxazoline ligands. *J. Org. Chem.* **68**, 4648–4656 (2003).
42. K. C. Harper, M. S. Sigman, Three-dimensional correlation of steric and electronic free energy relationships guides asymmetric propargylation. *Science* **333**, 1875–1878 (2011).
43. M. S. Sigman, K. C. Harper, E. N. Bess, A. Milo, The development of multidimensional analysis tools for asymmetric catalysis and beyond. *Acc. Chem. Res.* **49**, 1292–1301 (2016).
44. J. P. Reid, M. S. Sigman, Comparing quantitative prediction methods for the discovery of small-molecule chiral catalysts. *Nat. Rev. Chem* **2**, 290–305 (2018).
45. J. P. Reid, M. S. Sigman, Holistic prediction of enantioselectivity in asymmetric catalysis. *Nature* **571**, 343–348 (2019).
46. A. Verloop, J. Tipker, A comparative study of new steric parameters in drug design. *Pharmacochem. Libr.* **2**, 63–81 (1977).
47. K. C. Harper, E. N. Bess, M. S. Sigman, Multidimensional steric parameters in the analysis of asymmetric catalytic reactions. *Nat. Chem.* **4**, 366–374 (2012).
48. H. Clavier, S. P. Nolan, Percent buried volume for phosphine and *N*-heterocyclic carbene ligands: Steric properties in organometallic chemistry. *Chem. Commun.* **46**, 841–861 (2010).
49. L. Falivene, R. Credendino, A. Poater, A. Petta, L. Serra, R. Oliva, V. Scarano, L. Cavallo, SambVca 2. A web tool for analyzing catalytic pockets with topographic steric maps. *Organometallics* **35**, 2286–2293 (2016).
50. L. Falivene, Z. Cao, A. Petta, L. Serra, A. Poater, R. Oliva, V. Scarano, L. Cavallo, Towards the online computer-aided design of catalytic pockets. *Nat. Chem.* **11**, 872–879 (2019).
51. R. Zeng, C. Fu, S. Ma, Highly selective mild stepwise allylation of *N*-methoxybenzamides with allenes. *J. Am. Chem. Soc.* **134**, 9597–9600 (2012).
52. B.-S. Zhang, Y. Li, X.-Y. Gou, Z. Zhang, Y. An, X.-G. Wang, Y.-M. Liang, DMAP and PivOH-promoted amination/allenization reaction. *Chem. Commun.* **56**, 9202–9205 (2020).
53. G. Zhang, Y.-K. Song, F. Zhang, Z.-J. Xue, M.-Y. Li, G.-S. Zhang, B.-B. Zhu, J. Wei, C. Li, C.-G. Feng, G.-Q. Lin, Palladium-catalyzed allene synthesis enabled by β-hydrogen elimination from sp^2-carbon. *Nat. Commun.* **12**, 728 (2021).
54. A. D. Becke, Density-functional thermochemistry. III. The role of exact exchange. *J. Chem. Phys.* **98**, 5648–5652 (1993).
55. P. J. Stephens, F. J. Devlin, C. F. Chabalowski, M. J. Frisch, Ab initio calculation of vibrational absorption and circular dichroism spectra using density functional force fields. *J. Phys. Chem.* **98**, 11623–11627 (1994).
56. C. Lee, W. Yang, R. G. Parr, Development of the Colle-Salvetti correlation-energy formula into a functional of the electron density. *Phys. Rev. B Condens. Matter Mater. Phys.* **37**, 785–789 (1988).
57. M. J. Frisch, G. W. Trucks, H. B. Schlegel, G. E. Scuseria, M. A. Robb, J. R. Cheeseman, G. Scalmani, V. Barone, B. Mennucci, G. A. Petersson, H. Nakatsuji, M. Caricato, X. Li, H. P. Hratchian, A. F. Izmaylov, J. Bloino, G. Zheng, J. L. Sonnenberg, M. Hada, M. Ehara, K. Toyota, R. Fukuda, J. Hasegawa, M. Ishida, T. Nakajima, Y. Honda, O. Kitao, H. Nakai, T. Vreven, J. A. Montgomery Jr., J. E. Peralta, F. Ogliaro, M. Bearpark, J. J. Heyd, E. Brothers, K. N. Kudin, V. N. Staroverov, R. Kobayashi, J. Normand, K. Raghavachari, A. Rendell, J. C. Burant, S. S. Iyengar, J. Tomasi, M. Cossi, N. Rega, J. M. Millam, M. Klene, J. E. Knox, J. B. Cross, V. Bakken, C. Adamo, J. Jaramillo, R. Gomperts, R. E. Stratmann, O. Yazyev, A. J. Austin, R. Cammi, C. Pomelli, J. W. Ochterski, R. L. Martin, K. Morokuma, V. G. Zakrzewski, G. A. Voth, P. Salvador, J. J. Dannenberg, S. Dapprich, A. D. Daniels, Ö. Farkas, J. B. Foresman, J. V. Ortiz, J. Cioslowski, D. J. Fox, *Gaussian 09, Revision E.01* (Gaussian Inc., 2009).
58. F. M. Bickelhaupt, Understanding reactivity with Kohn–Sham molecular orbital theory: E2–SN2 mechanistic spectrum and other concepts. *J. Comput. Chem.* **20**, 114–128 (1999).
59. D. H. Ess, K. N. Houk, Distortion/interaction energy control of 1,3-dipolar cycloaddition reactivity. *J. Am. Chem. Soc.* **129**, 10646–10647 (2007).
60. D. H. Ess, K. N. Houk, Theory of 1,3-dipolar cycloadditions: Distortion/interaction and frontier molecular orbital models. *J. Am. Chem. Soc.* **130**, 10187–10198 (2008).
61. I. Fernández, F. M. Bickelhaupt, The activation strain model and molecular orbital theory: Understanding and designing chemical reactions. *Chem. Soc. Rev.* **43**, 4953–4967 (2014).
62. L. P. Wolters, F. M. Bickelhaupt, The activation strain model and molecular orbital theory. *WIREs Comp. Mol. Sci.* **5**, 324–343 (2015).
63. I. Fernández, F. M. Bickelhaupt, Deeper insight into the diels–alder reaction through the activation strain model. *Chem. Asian J.* **11**, 3297–3304 (2016).
64. F. M. Bickelhaupt, K. N. Houk, Analyzing reaction rates with the distortion/interaction-activation strain model. *Angew. Chem. Int. Ed.* **56**, 10070–10086 (2017).
65. T. M. Parker, L. A. Burns, R. M. Parrish, A. G. Ryno, C. D. Sherrill, Levels of symmetry adapted perturbation theory (SAPT). I. Efficiency and performance for interaction energies. *J. Chem. Phys.* **140**, 094106 (2014).
66. F. Weigenda, R. Ahlrichsb, Balanced basis sets of split valence, triple zeta valence and quadruple zeta valence quality for H to Rn: Design and assessment of accuracy. *Phys. Chem. Chem. Phys.* **7**, 3297–3305 (2005).

67. F. Weigenda, Accurate coulomb-fitting basis sets for H to Rn. *Phys. Chem. Chem. Phys.* **8**, 1057–1065 (2006).
68. R. M. Parrish, L. A. Burns, D. G. A. Smith, A. C. Simmonett, A. E. DePrince III, E. G. Hohenstein, U. Bozkaya, A. Y. Sokolov, R. Di Remigio, R. M. Richard, J. F. Gonthier, A. M. James, H. R. McAlexander, A. Kumar, M. Saitow, X. Wang, B. P. Pritchard, P. Verma, H. F. Schaefer III, K. Patkowski, R. A. King, E. F. Valeev, F. A. Evangelista, J. M. Turney, T. D. Crawford, C. D. Sherrill, Psi4 1.1: An open-source electronic structure program emphasizing automation, advanced libraries, and interoperability. *J. Chem. Theory Comput.* **13**, 3185–3197 (2017).
69. Z.-M. Zhang, B. Xu, Y. Qian, L. Wu, Y. Wu, L. Zhou, Y. Liu, J. Zhang, Palladium-catalyzed enantioselective reductive Heck reactions: Convenient access to 3,3-disubstituted 2,3-dihydrobenzofuran. *Angew. Chem. Int. Ed.* **57**, 10373–10377 (2018).
70. M. Dochnahl, G. C. Fu, Catalytic asymmetric cycloaddition of ketenes and nitroso compounds: Enantioselective synthesis of α-hydroxycarboxylic acid derivatives. *Angew. Chem. Int. Ed.* **48**, 2391–2393 (2009).
71. W. You, Y. Li, M. K. Brown, Stereoselective synthesis of all-carbon tetrasubstituted alkenes from in situ generated ketenes and organometallic reagents. *Org. Lett.* **15**, 1610–1613 (2013).
72. N. Jabri, A. Alexakis, J. F. Normant, Vinyl-copper derivatives 15^1: An efficient synthesis of polysubstituted conjugated dienes. *Tetrahedron Lett.* **23**, 1589–1592 (1982).
73. S. D. Huang, C. Shang, X. J. Zhang, Z. P. Liu, Material discovery by combining stochastic surface walking global optimization with a neural network. *Chem. Sci.* **8**, 6327–6337 (2017).
74. M. Ernzerhof, G. E. Scuseria, Assessment of the Perdew–Burke–Ernzerhof exchange-correlation functional. *J. Chem. Phys.* **110**, 5029–5036 (1999).
75. C. Adamo, V. Barone, Toward reliable density functional methods without adjustable parameters: The PBE0 model. *J. Chem. Phys.* **110**, 6158–6170 (1999).
76. S. Grimme, J. Antony, S. Ehrlich, H. Krieg, A consistent and accurate ab initio parametrization of density functional dispersion correction (DFT-D) for the 94 elements H-Pu. *J. Chem. Phys.* **132**, 154104 (2010).
77. M. Charlton, T. C. Griffith, G. R. Heyland, G. L. Wright, Total scattering cross sections for low-energy positrons in the molecular gases H_2, N_2, CO_2, O_2 and CH_4. *J. Phys. B. Atom. Mol. Phys.* **16**, 323–328 (1983).
78. D. Andrae, U. Häußermann, M. Dolg, H. Stoll, H. Preuß, Energy-adjusted ab initio pseudopotentials for the second and third row transition elements. *Theoretica. Chimica. Acta* **77**, 123–141 (1990).
79. A. V. Marenich, C. J. Christopher, D. G. Truhlar, Universal solvation model based on solute electron density and on a continuum model of the solvent defined by the bulk dielectric constant and atomic surface tensions. *J. Phys. Chem. B* **113**, 6378–6396 (2009).
80. T. Lu, Molclus program, version 1.9.9.9, www.keinsci.com/research/molclus.html [accessed 6 March 2022].
81. P. Pracht, F. Bohle, S. Grimme, Automated exploration of the low-energy chemical space with fast quantum chemical methods. *Phys. Chem. Chem. Phys.* **22**, 7169–7192 (2020).
82. C. Bannwarth, S. Ehlert, S. Grimme, GFN2-xTB—An accurate and broadly parametrized self-consistent tight-binding quantum chemical method with multipole electrostatics and density-dependent dispersion contributions. *J. Chem. Theory. Comput.* **15**, 1652–1671 (2019).
83. E. D. Glendening, C. R. Landis, F. Weinhold, Natural bond orbital methods. *WIREs Comput. Mol. Sci.* **2**, 1–42 (2012).
84. F. J. Weinhold, Natural bond orbital analysis: A critical overview of relationships to alternative bonding perspectives. *Comput. Chem.* **33**, 2363–2379 (2012).
85. A. E. Reed, R. B. Weinstock, F. J. Weinhold, Natural population analysis. *Chem. Phys.* **83**, 735–746 (1985).

Acknowledgments

Funding: We gratefully acknowledge the funding support of NSFC (22031004, 21921003), Shanghai Municipal Education Commission (20212308), and National Key R&D Program of China (2021YFF0701600). **Author contributions:** J.Z., S.M. and J.H. conceived the project and wrote the paper. J.H. performed the experiments and analyzed the data. S.L. and Z.L. conducted the computational studies. H.W. and J.W. helped in the synthesis of substrate **1**. H.Q. analyzed the data. All authors discussed the results and commented on the paper. **Competing interests:** The authors declare that they have no competing interests. **Data and materials availability:** All data needed to evaluate the conclusions in the paper are present in the paper and/or the Supplementary Materials.

Submitted 2 December 2022
Accepted 8 February 2023
Published 17 March 2023
10.1126/sciadv.adg1002